Swing-up control of a triple pendulum on a cart with experimental validation

authored by **T. Glück, A. Eder, and A. Kugi**

and published in *Automatica*.

Automation and Control Institute (ACIN)
Vienna University of Technology
Gusshausstrasse 27-29/E376
1040 Vienna, Austria

Internet: www.acin.tuwien.ac.at
E-mail: office@acin.tuwien.ac.at
Phone: +43 1 58801 37601
Fax: +43 1 58801 37699

Swing-up Control of a Triple Pendulum on a Cart with Experimental Validation ⋆

Tobias Glück [a], Andreas Eder [a], Andreas Kugi [a]

[a] *Automation and Control Institute, Vienna University of Technology, Gusshausstr. 27-29, 1040 Vienna, Austria*

Abstract

The swing-up control of a triple pendulum on a cart is presented, where the controller is based on a two-degrees-of-freedom scheme consisting of a nonlinear feedforward controller and an optimal feedback controller. The point-to-point transition task is treated as a nonlinear two-point boundary value problem with free parameters resulting from the suitably projected input-output dynamics. The main focus of the paper is on the experimental realization of the triple pendulum swing-up maneuver.

Key words: triple pendulum; swing-up; two-degrees-of-freedom control; constrained feedforward control; optimal feedback control.

1 Introduction

The inverted pendulum on a cart is a popular benchmark problem in control theory. The main reason for this is that it constitutes an underactuated system with a nonlinear, unstable and nonminimum-phase behavior and thus reveals many interesting system-theoretic properties.

In older literature, several contributions deal with the stabilization of single inverted pendulums, see, e.g., [2], [13]. Besides the rather simple stabilization task, the swing-up problem, where the pendulum is moved from the lower to the upper pendulum configuration, has attracted much attention, see, e.g., [19] and [20]. For double and triple pendulum configurations the stabilization task and even more the swing-up control is much more involved, in particular due to the limited rail length for the cart. In this context, most of the papers reported in the literature are restricted to pure simulation studies, see, e.g., [8] and [22], for the swing-up of an inverted double pendulum; [3], [12] and [18] for the stabilization of the inverted triple pendulum. In the last decade, the application of new control concepts in combination with the increasing computational power of the real-time hardware made it possible to also provide experiments for double and triple pendulum configurations. Thus, for instance [7] and [14] demonstrated the swing-up control of the double pendulum, and [6] presented the experimental verification of the side-stepping of an inverted triple pendulum on a cart in the upper configuration.

This paper is concerned with the design and experimental validation of the swing-up control of a triple pendulum on a cart. A video of the swing-up maneuver can be found on `http://www.acin.tuwien.ac.at/fileadmin/cds/videos/TP_Swing_up.wmv`.

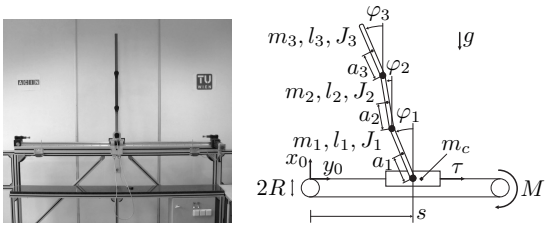

(a) Photograph of the test bench. (b) Schematics of the triple pendulum on a cart.

Figure 1. Test bench.

A photograph of the test bench under consideration [17] is depicted in Figure 1(a). Three pendulum arms are mounted on a horizontally movable cart. Incremental en-

⋆ This paper was not presented at any IFAC meeting. Corresponding author T. Glück. Tel. +43 1 58801-37678. Fax +43 1 58801-37699.

Email addresses: `glueck@acin.tuwien.ac.at` (Tobias Glück), `eder@acin.tuwien.ac.at` (Andreas Eder), `kugi@acin.tuwien.ac.at` (Andreas Kugi).

Post-print version of the article: T. Glück, A. Eder, and A. Kugi, "Swing-up control of a triple pendulum on a cart with experimental validation", *Automatica*, vol. 49, no. 3, pp. 801–808, 2013. DOI: 10.1016/j.automatica.2012.12.006
The content of this post-print version is identical to the published paper but without the publisher's final layout or copy editing.

coders at each joint measure the different angles between two adjacent arms and between the first arm and the cart, respectively, with a resolution of $4.395 \times 10^{-2}\,^{\circ}$. In order to keep the friction low, the signals are transmitted contactless via an optical connection from the joints to the control unit. The cart itself moves on a rail track and is driven via a toothed belt by a synchronous motor. An ideal subordinate angular speed controller is presumed, impressing the angular speed up to a maximum value of 3000 rpm. An additional incremental encoder on the synchronous motor is used to measure the position of the cart with a resolution of 6.836×10^{-5} m. The task under consideration is to design a controller with the angular speed of the synchronous motor as the control input in order to move the three pendulum arms from the downward to the upward position. This is also referred to as the swing-up maneuver of the triple pendulum on a cart.

In this paper, the control problem is accomplished by means of a two-degrees-of-freedom control structure. First, the mathematical model of the considered system is derived in Section 2. A systematic parameter identification procedure is carried out in Section 3. The development of the two-degrees-of-freedom control concept with a *nonlinear feedforward controller*, a time-variant *Riccati controller* and a state observer in form of an *Extended Kalman Filter* is demonstrated in Section 4. The key challenge of the swing-up maneuver is the design of an appropriate feedforward controller. This is realized by a reformulation of the systems' dynamics in input-output coordinates. A suitable projection of the input-output dynamics allows to directly incorporate the given output constraints and an appropriate input parametrization facilitates the solvability of the resulting two-point boundary value problem with free parameters. Experimental results, shown in Section 5, demonstrate the performance of the overall control strategy.

2 Mathematical Model

At first, the systematic derivation of the equations of motion of the triple pendulum on a cart by means of the *Lagrange formalism* is shown. A schematic diagram of the triple pendulum on a cart is sketched in Figure 1(b). The cart position s and the angles φ_i, $i = 1, 2, 3$ between the pendulum arms and the vertical axis are chosen as generalized coordinates and summarized in the vector $\mathbf{q}^{\mathsf{T}} = [\varphi_1\, \varphi_2\, \varphi_3\, s] = [q_1\, q_2\, q_3\, q_4]$. The distance of the center of gravity of each pendulum arm to the corresponding joint is denoted by a_i, $i = 1, 2, 3$. Furthermore, m_c describes the mass of the cart and the pendulum arms have the lengths l_i, the masses m_i and the moments of inertia J_i. The synchronous motor generates the motor moment M which results in a control force $\tau = M/R$ acting on the cart by neglecting the elasticity of the toothed drive belt. Here, R denotes the radius of the toothed belt disk.

2.1 Equations of motion

The equations of motion are derived by means of the *Lagrange formalism*, see, e.g., [15],

$$\frac{\mathrm{d}}{\mathrm{d}t}\frac{\partial}{\partial \dot{q}_k}\mathcal{L} - \frac{\partial}{\partial q_k}\mathcal{L} + \frac{\partial}{\partial \dot{q}_k}\mathcal{R} = \tau\,\delta_{k4}, \quad k = 1, \ldots, 4, \tag{1}$$

with the *Lagrangian* $\mathcal{L} = \mathcal{T} - \mathcal{V}$ as the difference between the kinetic energy $\mathcal{T}$ and the potential energy $\mathcal{V}$, the *Rayleigh dissipation function* $\mathcal{R}$ accounting for the viscous friction and the external control force τ. Furthermore, $\delta_{ij} = 1$ for $i = j$ and $\delta_{ij} = 0$ for $i \neq j$ denotes the Kronecker-Delta. The vector from the origin of the inertial frame $(x_0\, y_0)$ to the center of gravity of the individual pendulum arms take the form

$$\mathbf{p}_{c1} = \begin{bmatrix} s - a_1 \sin\varphi_1 \\ a_1 \cos\varphi_1 \end{bmatrix}, \mathbf{p}_{c2} = \begin{bmatrix} s - l_1 \sin\varphi_1 - a_2 \sin\varphi_2 \\ l_1 \cos\varphi_1 + a_2 \cos\varphi_2 \end{bmatrix},$$
$$\mathbf{p}_{c3} = \begin{bmatrix} s - l_1 \sin\varphi_1 - l_2 \sin\varphi_2 - a_3 \sin\varphi_3 \\ l_1 \cos\varphi_1 + l_2 \cos\varphi_2 + a_3 \cos\varphi_3 \end{bmatrix}. \tag{2}$$

Thus, the kinetic energy $\mathcal{T}$ consists of the translational part of the cart $\mathcal{T}_c = \frac{1}{2} m_c \dot{s}^2$ and the translational and rotational part of the pendulum arms $\mathcal{T}_p = \frac{1}{2}\sum_{j=1}^{3} m_j \dot{\mathbf{p}}_{cj}^{\mathsf{T}} \dot{\mathbf{p}}_{cj} + \frac{1}{2}\sum_{j=1}^{3} J_j \omega_j^2$ with the angular velocities $\omega_i = \dot{\varphi}_i$, $i = 1, 2, 3$. The potential energy $\mathcal{V}$ due to the gravitational field reads as $\mathcal{V} = g\,(m_1 \mathbf{p}_{c1,2} + m_2 \mathbf{p}_{c2,2} + m_3 \mathbf{p}_{c3,2})$, with the acceleration of gravity g. *Rayleigh's dissipation function* $\mathcal{R}$ is used to incorporate the viscous friction of the joints $\mathcal{R} = \frac{1}{2} d_1 \omega_1^2 + \frac{1}{2} d_2\,(\omega_2 - \omega_1)^2 + \frac{1}{2} d_3\,(\omega_3 - \omega_2)^2$, with the viscous friction coefficients d_i, $i = 1, 2, 3$. The friction of the cart is neglected since the cart dynamics will be simplified, as will be shown in Section 2.2, due to the assumption of an ideal subordinate angular velocity controller of the synchronous motor. In vector notation, the equations of motion due to (1) read as

$$\mathbf{D}(\mathbf{q})\ddot{\mathbf{q}} + \mathbf{C}(\mathbf{q}, \dot{\mathbf{q}})\dot{\mathbf{q}} + \mathbf{G}\dot{\mathbf{q}} + \mathbf{g}(\mathbf{q}) = \boldsymbol{\tau}, \tag{3}$$

with the positive definite mass matrix $\mathbf{D}(\mathbf{q})$, the Coriolis matrix $\mathbf{C}(\mathbf{q}, \dot{\mathbf{q}})$, the damping matrix $\mathbf{G}$, the vector of gravity $\mathbf{g}(\mathbf{q})$ and the control force $\boldsymbol{\tau}^{\mathsf{T}} = [\mathbf{0}_{1\times 3}\, \tau]$.

2.2 Subordinate angular velocity controller

As already mentioned before, the synchronous motor is controlled by a subordinate angular velocity controller, which is assumed to be ideal. Therefore, the reaction of the pendulum arms on the cart can be neglected and the acceleration of the cart $\ddot{s}$ is chosen as the new control input u. This brings about that the last row in the equations of motion (3) must be replaced by $\ddot{s} = u$. For implementation purposes, u is integrated with respect

Post-print version of the article: T. Glück, A. Eder, and A. Kugi, "Swing-up control of a triple pendulum on a cart with experimental validation", *Automatica*, vol. 49, no. 3, pp. 801–808, 2013. DOI: 10.1016/j.automatica.2012.12.006
The content of this post-print version is identical to the published paper but without the publisher's final layout or copy editing.

to time in order to obtain the reference cart velocity $\dot{s}_d$ which in turn serves as the input for the subordinate angular velocity controller. Thus, the equations of motion (3) with the ideal subordinate velocity controller take the form

$$\begin{aligned} \check{\mathbf{D}}_{\varphi\varphi}(\boldsymbol{\varphi})\ddot{\boldsymbol{\varphi}} = &- \check{\mathbf{D}}_{\varphi s}(\boldsymbol{\varphi})\ddot{s} - \check{\mathbf{C}}_{\varphi\varphi}(\boldsymbol{\varphi},\dot{\boldsymbol{\varphi}})\dot{\boldsymbol{\varphi}}, \\ &- \check{\mathbf{G}}_{\varphi\varphi}\dot{\boldsymbol{\varphi}} - \check{\mathbf{g}}_{\varphi\varphi}(\boldsymbol{\varphi}), \\ \ddot{s} = &\, u, \end{aligned} \tag{4}$$

with the matrices and vectors $\check{\mathbf{D}}_{\varphi\varphi}$, $\check{\mathbf{D}}_{\varphi s}$, $\check{\mathbf{C}}_{\varphi\varphi}$, $\check{\mathbf{G}}_{\varphi\varphi}$, $\check{\mathbf{g}}_{\varphi\varphi}$ and $\boldsymbol{\varphi}^{\mathsf{T}} = [\varphi_1\, \varphi_2\, \varphi_3]$. By introducing the state vector $\mathbf{x}^{\mathsf{T}} = [\mathbf{q}\, \dot{\mathbf{q}}]$ the equations of motion of the triple pendulum may be written in the input-affine system representation

$$\dot{\mathbf{x}} = \mathbf{f}(\mathbf{x}) + \mathbf{g}(\mathbf{x})u, \quad \mathbf{x}(0) = \mathbf{x}_0, \tag{5}$$

with $\mathbf{f}^{\mathsf{T}}(\mathbf{x}) = \left[\dot{\mathbf{q}}^{\mathsf{T}}\, \mathbf{F}_0^{\mathsf{T}}(\boldsymbol{\varphi},\dot{\boldsymbol{\varphi}})\, 0\right]$, $\mathbf{g}^{\mathsf{T}}(\mathbf{x}) = \left[\mathbf{0}_{1\times 4}\, \mathbf{F}_1^{\mathsf{T}}(\boldsymbol{\varphi})\, 1\right]$ and

$$\begin{aligned} \mathbf{F}_0(\boldsymbol{\varphi},\dot{\boldsymbol{\varphi}}) &= -\check{\mathbf{D}}_{\varphi\varphi}^{-1}(\boldsymbol{\varphi})\left(\check{\mathbf{C}}_{\varphi\varphi}(\boldsymbol{\varphi},\dot{\boldsymbol{\varphi}})\dot{\boldsymbol{\varphi}} + \check{\mathbf{G}}_{\varphi\varphi}\dot{\boldsymbol{\varphi}} + \check{\mathbf{g}}_{\varphi\varphi}(\boldsymbol{\varphi})\right), \\ \mathbf{F}_1(\boldsymbol{\varphi}) &= -\check{\mathbf{D}}_{\varphi\varphi}^{-1}(\boldsymbol{\varphi})\check{\mathbf{D}}_{\varphi s}(\boldsymbol{\varphi}). \end{aligned} \tag{6}$$

2.3 Equilibrium points

The triple pendulum model (5) exhibits in total eight equilibrium points for a fixed cart position $s_{\mathrm{sp}} = 0$ and control input $u_{\mathrm{sp}} = 0$. The equilibrium points can be simply calculated from (4) by setting $\boldsymbol{g}_{\varphi\varphi}(\boldsymbol{\varphi}) = \mathbf{0}$. In the following, the swing-up maneuver is only concerned with the setpoint transition from the stretched out pendulum arm in the downward position $\boldsymbol{\varphi}_0^{\mathsf{T}} = [\pi\, \pi\, \pi]$ to the upward position $\boldsymbol{\varphi}_T^{\mathsf{T}} = [0\, 0\, 0]$. At this point it is worth noting that the control approach being subsequently presented in principle also applies to the setpoint transition between other equilibrium points.

3 Parameter identification

One of the sticking points for a successful realization of the swing-up maneuver is the exact parametrization of the model. Even a small parameter mismatch will have an immense influence on the calculation of the feedforward trajectory and thus on the overall performance. The direct determination of 15 parameters, five parameters $(m_i, l_i, a_i, d_i, J_i)$ for each pendulum arm, is quite difficult. The identification task, however, is significantly simplified if, in a first step, the parameters of the pendulum arms are individually determined. Afterwards, in a second step, the friction coefficients $d_i,\ i = 1, 2, 3$ have to be identified once again. This is necessary because in the triple pendulum configuration the normal forces acting on the bearings are different. Summarizing, the identification strategy can be subdivided into three steps:

(i) Five parameters $(m_i, l_i, a_i, d_i, J_i)$ have to be identified for each pendulum arm. The mass m_i, the pendulum arm length l_i and the distance a_i of the center of gravity to the corresponding joint are directly measurable. They are determined as $m_1 = 0.876\,\mathrm{kg}, m_2 = 0.938\,\mathrm{kg}, m_3 = 0.553\,\mathrm{kg},\ a_1 = 0.215\,\mathrm{m}, a_2 = 0.269\,\mathrm{m}, a_3 = 0.226\,\mathrm{m},\ l_1 = 0.323\,\mathrm{m}, l_2 = 0.419\,\mathrm{m}$ and $l_3 = 0.484\,\mathrm{m}$. (ii) The parameters J_i and d_i are determined by a parametric linear *Least-Squares* identification for each single pendulum. The equation of motion of the single pendulum for fixed cart position and zero input, i.e. $u = 0$, is given by, see, e.g., [21],

$$\dot{\omega} = \theta_a \sin(\varphi) + \theta_b \omega, \quad \omega(0) = \omega_0. \tag{7}$$

with parameters $\theta_a = \frac{m_i a_i g}{m_i a_i^2 + J_i}$ and $\theta_b = \frac{-d_i}{m_i a_i^2 + J_i}$. Thus, (7) constitutes a parametric linear identification problem of the form $y = \mathbf{s}^{\mathsf{T}}\boldsymbol{\theta}_1$ with output $y = \dot{\omega}$, regressor $\mathbf{s}^{\mathsf{T}} = [\omega\, \sin(\varphi)]$ and parameter vector $\boldsymbol{\theta}_1^{\mathsf{T}} = [\theta_a\, \theta_b]$. Hence, N measurements yield the overdetermined linear system of equations $\mathbf{y} = \mathbf{S}\boldsymbol{\theta}$ featuring the optimal solution $\hat{\boldsymbol{\theta}}_1 = \left(\mathbf{S}^{\mathsf{T}}\mathbf{S}\right)^{-1}\mathbf{S}^{\mathsf{T}}\mathbf{y}$ in the *Least-Squares* sense, see, e.g., [11]. Based on the knowledge of the parameters m_i, l_i and a_i, the remaining parameters J_i and d_i from (7) are calculated by $J_i = -\frac{m_i\, a_i\, (\theta_a\, a_i - g)}{\theta_a}$ and $d_i = -\frac{\theta_b\, m_i\, a_i\, g}{\theta_a}$. Each pendulum arm was mounted on the cart and separately identified. For this a test by free oscillations in the time interval $t \in [0, T_m]$ in the lower pendulum configuration for a fixed cart position was performed. The identification results of the individual pendulum arms are depicted in Figure 2. (iii) Finally, a parametric nonlinear *Least-Squares* identification

$$\begin{aligned} \min_{\boldsymbol{\theta}_2} J(\boldsymbol{\theta}_2) &= \frac{1}{T_m}\int_0^{T_m}\sum_{i=0}^{3}\left(\varphi_i(t;\boldsymbol{\theta}_2) - \varphi_{i,m}\right)^2 \mathrm{d}t \\ \text{s.t.} \quad \dot{\mathbf{x}} &= \mathbf{f}(\mathbf{x};\boldsymbol{\theta}_2) + \mathbf{g}(\mathbf{x};\boldsymbol{\theta}_2)u, \quad \mathbf{x}(0) = \mathbf{x}_0, \\ \boldsymbol{\theta}_2^{\mathsf{T}} &= [d_1\, d_2\, d_3],\ d_i \geq 0,\ i = 1, 2, 3, \end{aligned} \tag{8}$$

where $\varphi_{i,m}$ are the measurements of the angles φ_i over the time interval T_m, was carried out in order to capture the viscous friction in the triple pendulum configuration. Here, $\mathbf{f}$ and $\mathbf{g}$ are identical to (5), just with a little abuse of notation the argument $(\cdot;\boldsymbol{\theta}_2)$ should explicitly indicate the dependence on the parameter vector $\boldsymbol{\theta}_2$. The identification procedure was performed in MATLAB by means of the function `fmincon` using the sequential quadratic programming method in combination with the ordinary differential equations solver `ode15s`. Figure 3 shows the identification results obtained from measurements of the side-stepping in the lower triple pendulum configuration. Summarizing, the last two identification steps provide the remaining model parameters $J_1 = 0.013\,\mathrm{Nms}^2, J_2 = 0.024\,\mathrm{Nms}^2, J_3 = 0.018\,\mathrm{Nms}^2$, $d_1 = 0.215\,\mathrm{Nms}, d_2 = 0.002\,\mathrm{Nms}$ and $d_3 = 0.002\,\mathrm{Nms}$.

Post-print version of the article: T. Glück, A. Eder, and A. Kugi, "Swing-up control of a triple pendulum on a cart with experimental validation", *Automatica*, vol. 49, no. 3, pp. 801–808, 2013. DOI: 10.1016/j.automatica.2012.12.006
The content of this post-print version is identical to the published paper but without the publisher's final layout or copy editing.

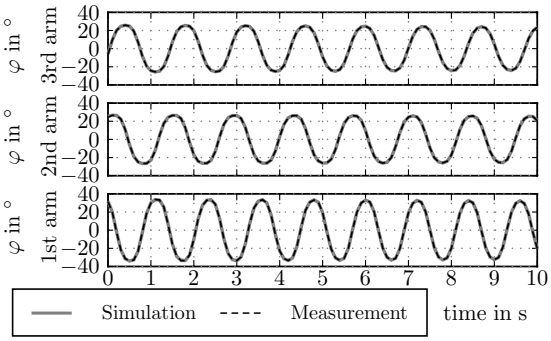

Figure 2. Comparison of the simulation and measurement results of the parametric linear identification by means of free oscillation tests of the individual pendulum arms.

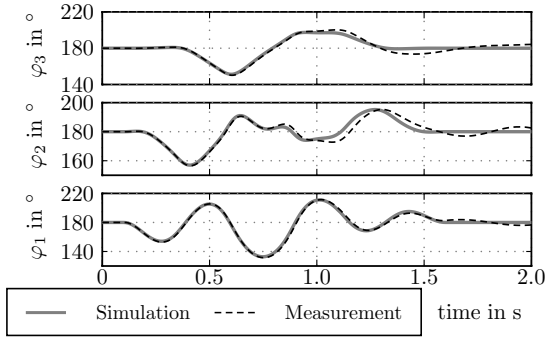

Figure 3. Comparison of the simulation and measurement results of the parametric nonlinear identification by means of measurements of the uncontrolled side-stepping in the lower triple pendulum configuration.

4 Control strategy for the swing-up maneuver

The swing-up control strategy is based on the two-degrees-of-freedom control structure shown in Figure 4.

4.1 Two-degrees-of-freedom control structure

The key benefit of this design structure is the possibility to separately adjust the tracking and the disturbance behavior. A trajectory generator provides the desired output trajectory $y^*(t)$ for calculating the feedforward control $u^*(t)$. Deviations of the real system from the reference trajectory $\mathbf{x}^*$ due to model uncertainties or disturbances are suppressed by means of a feedback controller. The control input $u(t) = u^*(t) + \Delta u$ consists of the feedforward part $u^*(t)$ and the feedback part Δu, whereas the quantities $\mathbf{y}_m$ are made available by measurements. Non-measurable states may be reconstructed by means of an observer.

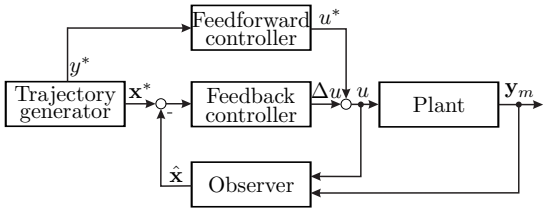

Figure 4. Two-degrees-of-freedom control structure.

4.2 Feedforward controller design

The mathematical model (5) of the triple pendulum, with the cart position $y = s$ as the output and the corresponding relative degree $r = 2$ can be written in *Byrnes-Isidori normal form*, see [9],

$$\ddot{y} = u, \tag{9a}$$
$$\ddot{\boldsymbol{\eta}} = \boldsymbol{F}_0(\boldsymbol{\eta}, \dot{\boldsymbol{\eta}}) + \boldsymbol{F}_1(\boldsymbol{\eta})u, \tag{9b}$$

where $\boldsymbol{\eta}^\mathsf{T} = \boldsymbol{\varphi}^\mathsf{T} = [\varphi_1\, \varphi_2\, \varphi_3]$ and $\dot{\boldsymbol{\eta}}^\mathsf{T} = \dot{\boldsymbol{\varphi}}^\mathsf{T} = [\omega_1\, \omega_2\, \omega_3]$ represent the state variables of the internal dynamics and $\boldsymbol{F}_i$, $i = 0, 1$ is according to (6). The swing-up maneuver performed in a finite transition time T corresponds to a point-to-point motion from the initial setpoint

$$y(0) = s_0 = 0, \quad \dot{y}(0) = 0, \tag{10a}$$
$$\boldsymbol{\eta}^\mathsf{T}(0) = \boldsymbol{\eta}_0^\mathsf{T} = [\pi\, \pi\, \pi]\,, \dot{\boldsymbol{\eta}}(0) = \dot{\boldsymbol{\eta}}_0 = \mathbf{0}, \tag{10b}$$

to the terminal setpoint

$$y(T) = s_T = 0, \quad \dot{y}(T) = 0, \tag{11a}$$
$$\boldsymbol{\eta}^\mathsf{T}(T) = \boldsymbol{\eta}_T^\mathsf{T} = [0\,0\,0]\,, \dot{\boldsymbol{\eta}}(T) = \dot{\boldsymbol{\eta}}_T = \mathbf{0}. \tag{11b}$$

The output and its time-derivatives up to the order $r = 2$ have to satisfy the box-constraints

$$y^{(i)}(t) \in \left[y_i^-, y_i^+\right], \quad i \in \{0, 1, 2\} \tag{12}$$

with $y_i^- < 0 < y_i^+$ and $-y_i^- = y_i^+$. The differential equations (9) in combination with the boundary conditions (10) - (11) and the constraints (12) form a nonlinear, constrained two-point boundary value problem for the states $y(t)$, $\dot{y}(t)$ and $\boldsymbol{\eta}(t)$, $\dot{\boldsymbol{\eta}}(t)$ depending on the input $u(t)$. The determination of the desired trajectories $y^*(t)$, $\dot{y}^*(t)$, $\boldsymbol{\eta}^*(t)$, $\dot{\boldsymbol{\eta}}^*(t)$ and the corresponding control input $u^*(t)$ is the main objective of the feedforward control design.

4.2.1 Output-constrained feedforward control design

The design approach presented here follows [5]. The basic idea is the successive incorporation of the output constraints in a new, projected system representation by

Post-print version of the article: T. Glück, A. Eder, and A. Kugi, "Swing-up control of a triple pendulum on a cart with experimental validation", *Automatica*, vol. 49, no. 3, pp. 801–808, 2013. DOI: 10.1016/j.automatica.2012.12.006
The content of this post-print version is identical to the published paper but without the publisher's final layout or copy editing.

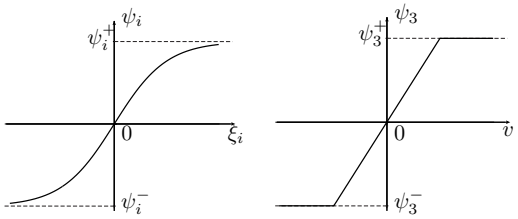

(a) Smooth saturation functions $\psi_i(\xi_i, \psi_i^\pm)$ with new states ξ_i, $i \in \{1, 2\}$.

(b) Ramp-shaped saturation function $\psi_3(v, \psi_3^\pm)$ with new input v.

Figure 5. Saturation functions with the limits ψ_i^- and ψ_i^+ for $i \in \{1, 2, 3\}$.

introducing saturation functions. The constraints of the desired output trajectory y^* are considered by introducing the saturation function, see Figure 5(a),

$$y^* = \psi_1(\xi_1, \psi_1^\pm), \tag{13}$$

with the new state ξ_1. Differentiating (13) once and twice with respect to the time yields

$$\dot{y}^* = \frac{\partial \psi_1}{\partial \xi_1}\dot{\xi}_1 \quad \text{and} \quad \ddot{y}^* = \frac{\partial^2 \psi_1}{\partial \xi_1^2}\dot{\xi}_1^2 + \frac{\partial \psi_1}{\partial \xi_1}\ddot{\xi}_1. \tag{14}$$

With this, the new saturation functions ψ_2 and ψ_3 are introduced

$$\dot{\xi}_1 = \psi_2\big(\xi_2, \psi_2^\pm(\xi_1)\big) \text{ and } \dot{\xi}_2 = \psi_3\big(v, \psi_3^\pm(\xi_1, \xi_2)\big), \tag{15}$$

with another new state ξ_2 and the new input v. Now, the system (15) represents a new, projected system fulfilling the output constraints (12).

Determination of the saturation limits

Obviously, the constraint $y^* \in \left[y_0^-, y_0^+\right]$ is satisfied if the saturation limits are chosen as

$$\psi_1^\pm = y_0^\pm. \tag{16}$$

In order to determine the saturation limits $\psi_i^\pm$, $i = 2, 3$, the constraints $\mathrm{d}^i y^*/\mathrm{d}t^i \in \left[y_i^-, y_i^+\right]$, $i = 1, 2$ have to be satisfied. It will be assumed in the subsequent consideration that the saturation functions $\psi_i(\xi_i, \psi_i^\pm)$, $i = 1, 2$, are strictly monotonically increasing, i.e. $\partial \psi_i / \partial \xi_i > 0$. The inequalities $y_i^- \le \mathrm{d}^i y^*/\mathrm{d}t^i \le y_i^+$, $i = 1, 2$ in combination with (14) and (15) may be rearranged in the form

$$y_1^- \le \frac{\partial \psi_1}{\partial \xi_1}\psi_2 \le y_1^+, \tag{17a}$$

$$y_2^- \le \frac{\partial^2 \psi_1}{\partial \xi_1^2}\psi_2^2 + \frac{\partial \psi_1}{\partial \xi_1}\left[\frac{\partial \psi_2}{\partial \xi_2}\psi_3 + \frac{\partial \psi_2}{\partial \xi_1}\psi_2\right] \le y_2^+, \tag{17b}$$

and thus the limits of the saturation function ψ_2 and ψ_3 can be calculated as

$$\psi_2^\pm(\xi_1) = y_1^\pm \left[\frac{\partial \psi_1}{\partial \xi_1}\right]^{-1}, \tag{18a}$$

$$\psi_3^\pm(\xi_1, \xi_2) = y_2^\pm \left[\frac{\partial \psi_1}{\partial \xi_1}\frac{\partial \psi_2}{\partial \xi_2}\right]^{-1} - \left[\frac{\partial^2 \psi_1}{\partial \xi_1^2}\psi_2^2 + \frac{\partial \psi_1}{\partial \xi_1}\frac{\partial \psi_2}{\partial \xi_1}\psi_2\right]\left[\frac{\partial \psi_1}{\partial \xi_1}\frac{\partial \psi_2}{\partial \xi_2}\right]^{-1}. \tag{18b}$$

It is clear from (18) that $\psi_i^\pm$, $i = 2, 3$ not only depend on $y_i^\pm$, $i = 1, 2$ but also on the new states ξ_i, $i = 1, 2$.

Calculation of the boundary values

The boundary values of the state ξ_1 are obtained by inverting the sigmoid saturation function (13)

$$\xi_{1,0} = \psi_1^{-1}(s_0, \psi_1^\pm) \quad \text{and} \quad \xi_{1,T} = \psi_1^{-1}(s_T, \psi_1^\pm). \tag{19}$$

The remaining boundary conditions $\xi_{2,0}$ and $\xi_{2,T}$ are determined from stationary considerations. Since the output y approaches a constant value in steady state and thus its time derivatives vanish, the system can be described by the stationary equation

$$0 = \psi_2\big(\xi_2, \psi_2^\pm(\xi_1)\big) \tag{20}$$

which, for symmetric constraints, i.e. $\left|\psi_2^-(\xi_1)\right| = \left|\psi_2^+(\xi_1)\right|$, yields the boundary conditions

$$\xi_{2,0} = \psi_2^{-1}\big(0, \psi_2^\pm(\xi_{1,0})\big) = 0 \tag{21a}$$

$$\xi_{2,T} = \psi_2^{-1}\big(0, \psi_2^\pm(\xi_{1,T})\big) = 0, \tag{21b}$$

since the saturation function (20) passes through the origin.

Saturation functions

As previously mentioned, the first $r = 2$ saturation functions $\psi_i(\xi_i, \psi_i^\pm)$, $i = 1, 2$ are assumed to be strictly monotonically increasing, i.e. $\partial \psi_i / \partial \xi_i > 0$, $i = 1, 2$. An appropriate sigmoid setup function, depicted in Figure 5(a), is proposed in [5], i.e.

$$\psi_i(\xi_i, \psi_i^\pm) = \psi_i^+ - \frac{\psi_i^+ - \psi_i^-}{1 + \exp(m\xi_i)}, \quad i = 1, 2. \tag{22}$$

The parameter m adjusts the slope at $\xi_i = 0$ and is set to $m = 4/(\psi_i^+ - \psi_i^-)$ in order to assure $\partial \psi_i / \partial \xi_i = 1$ at $\xi_i = 0$. According to the procedure presented above, the last saturation function $\psi_3(v, \psi_3^\pm)$ need not fulfill

Post-print version of the article: T. Glück, A. Eder, and A. Kugi, "Swing-up control of a triple pendulum on a cart with experimental validation", *Automatica*, vol. 49, no. 3, pp. 801–808, 2013. DOI: 10.1016/j.automatica.2012.12.006
The content of this post-print version is identical to the published paper but without the publisher's final layout or copy editing.

any differentiability requirements, which is why a ramp-shaped saturation function, see Figure 5(b),

$$\psi_3\big(v,\psi_3^{\pm}\big)=\begin{cases}\psi_3^{+} & \text{for} \quad v>\psi_3^{+}\\ v & \text{for} \quad v\in\big[\psi_3^{-},\psi_3^{+}\big]\\ \psi_3^{-} & \text{for} \quad v<\psi_3^{-}\end{cases} \tag{23}$$

may be used.

Setup function

The projected input-output dynamics (15) in combination with the internal dynamics (9b) and the boundary conditions (10b), (11b), (19) and (21) form the new two-point boundary value problem which is over-determined with $n=8$ first-order differential equations for the $2n=16$ boundary conditions. Using the trigonometric setup function

$$v=\Phi(t,\boldsymbol{p})=\sum_{i=1}^{n}p_i\sin\left(\frac{h_i\pi t}{T}\right) \tag{24}$$

for the new input v with $n=8$ free parameters $\boldsymbol{p}=(p_1,\ldots,p_8)$ and $h_i\in\mathbb{N}^{+}\backslash\{0\}$, $i=1,\ldots,n$ for $h_i\neq h_j,\forall i\neq j$ which satisfies the boundary conditions

$$\Phi(0,\boldsymbol{p})=\Phi(T,\boldsymbol{p})=0, \tag{25}$$

the problem is transformed into a well-defined two-point boundary value problem. The choice of the setup function $\Phi(t,\boldsymbol{p})$ and of the transition time T is a crucial point within this design methodology, because it somehow restricts the space of possible solutions.

Resulting two-point boundary value problem

The determination of the feedforward control u^* requires the solution of the internal dynamics (9b) augmented with the projected input-output dynamics (15)

$$\begin{aligned}\dot{\xi}_1&=\psi_2\big(\xi_2,\psi_2^{\pm}(\xi_1)\big),\\ \dot{\xi}_2&=\psi_3\big(\Phi(t,\boldsymbol{p}),\psi_3^{\pm}(\xi_1,\xi_2)\big),\\ \ddot{\boldsymbol{\eta}}^*&=\boldsymbol{F}_0(\boldsymbol{\eta}^*,\dot{\boldsymbol{\eta}}^*)+\boldsymbol{F}_1(\boldsymbol{\eta}^*)\,u^*,\end{aligned} \tag{26}$$

with the inverse of the input-output dynamics $u^*=\ddot{y}^*$, cf. (9a). Here, it is simply the second time-derivative of the output according to (14),(15)

$$\begin{aligned}u^*=&\frac{\partial^2\psi_1}{\partial\xi_1^2}\psi_2^2\\ &+\frac{\partial\psi_1}{\partial\xi_1}\left[\frac{\partial\psi_2}{\partial\xi_1}\psi_2+\frac{\partial\psi_2}{\partial\xi_2}\psi_3\big(\Phi(t,\boldsymbol{p}),\psi_3^{\pm}(\xi_1,\xi_2)\big)\right],\end{aligned}$$

with the setup function $\Phi(t,\boldsymbol{p})$ from (24) depending on the free parameters. Furthermore, a solution must satisfy the boundary conditions (10b), (11b), (19) and (21) with the saturation limits from (16) and (18). The desired output trajectory $y^*(t)$ and its time-derivative $\dot{y}^*(t)$ are determined by the algebraic equations (13)-(15).

4.2.2 *Numerical solution of the two-point boundary value problem*

The numerical solution of the nonlinear two-point boundary value problem with free parameters (26) is performed in MATLAB by means of the solver `bvp5c`. The function `bvp5c` implements a finite difference method, in particular a collocation method, see [10], that controls a scaled residual and the true error and adapts the mesh grid. The function `bvp5c` is able to solve, due to its algebraic solution technique, both stable and unstable sets of differential equations in a numerically stable manner. As has already been noted, any setup function $\Phi(t,\boldsymbol{p})$ and transition time T fulfilling the boundary conditions could have been used. However, the particular choice restricts the space of possible solutions. The setup function with its free parameters, the transition time and the constraints have to define a nonempty set of possible solutions. If this is not the case, the numerical solver will not converge to a solution. Furthermore, the function `bvp5c` requires an initial guess for the solution and an initial mesh grid. The solver may not find a solution if the initial guess does not adequately represent the behavior of the system, see, e.g., [10]. As the adequate initial guess is not easy to find, there is a need for a systematic solution procedure. The two-point boundary value problem (26) is therefore numerically solved in a sequential procedure that can be summarized as follows: A linear interpolation between the boundary conditions (10) and (11) on a uniform mesh of $N=200$ grid points at the time steps $t_j=jT_j$, $j=0,1,\ldots,N$, $T_j=T/N$ serves as initial guess for the trajectories $y^*(t_j)$, $\dot{y}^*(t_j)$, $\boldsymbol{\eta}^*(t_j)$ and $\dot{\boldsymbol{\eta}}^*(t_j)$. The initial guess for the parameters is set to $\boldsymbol{p}=\boldsymbol{0}$. Then the problem is solved for

(i) a sequence of setup functions (24) with $h_i\in\{1,\ldots,\gamma\}$, $\gamma\in\mathbb{N}^{+}\backslash\{0\}$, $i=1,2,\ldots,n$ for $h_i\neq h_j,\forall i\neq j$ and
(ii) a uniform sequence of transition times $T\in\{T_{\text{start}},\ldots,T_{\text{end}}\}$ with $T_{\text{start}}<T_{\text{end}}$

monitoring the Jacobian and the true error. The computing time is decreased by using the PARALLEL TOOLBOX from MATLAB. Figure 6 shows a solution for the swing-up maneuver following this procedure for the output constraints $y_0^{+}=-y_0^{-}=0.7\,\text{m}$, $y_1^{+}=-y_1^{-}=3\,\text{m/s}$ and $y_2^{+}=-y_2^{-}=22\,\text{m/s}^2$. The transition time is $T=3.5\,\text{s}$ and the setup function (24) with coefficients $h_i=i$ for $i\in\{2,3,4,5,6,7,8,9\}$ was found. In order to illustrated this motion, Figure 7 shows time-discrete snapshots of the pendulum for this swing-up maneuver.

Post-print version of the article: T. Glück, A. Eder, and A. Kugi, "Swing-up control of a triple pendulum on a cart with experimental validation", *Automatica*, vol. 49, no. 3, pp. 801–808, 2013. DOI: 10.1016/j.automatica.2012.12.006
The content of this post-print version is identical to the published paper but without the publisher's final layout or copy editing.

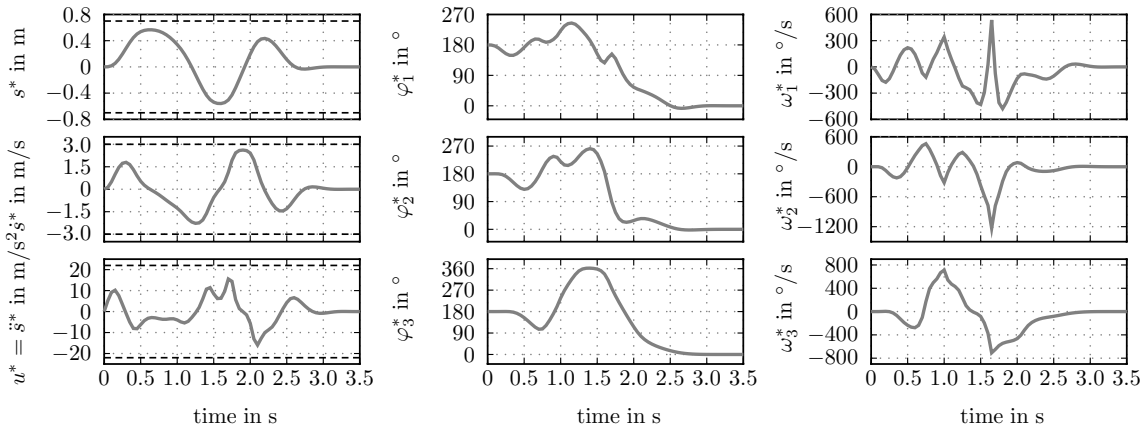

Figure 6. Numerical results for the swing-up maneuver with a transition time of $T = 3.5\,\mathrm{s}$.

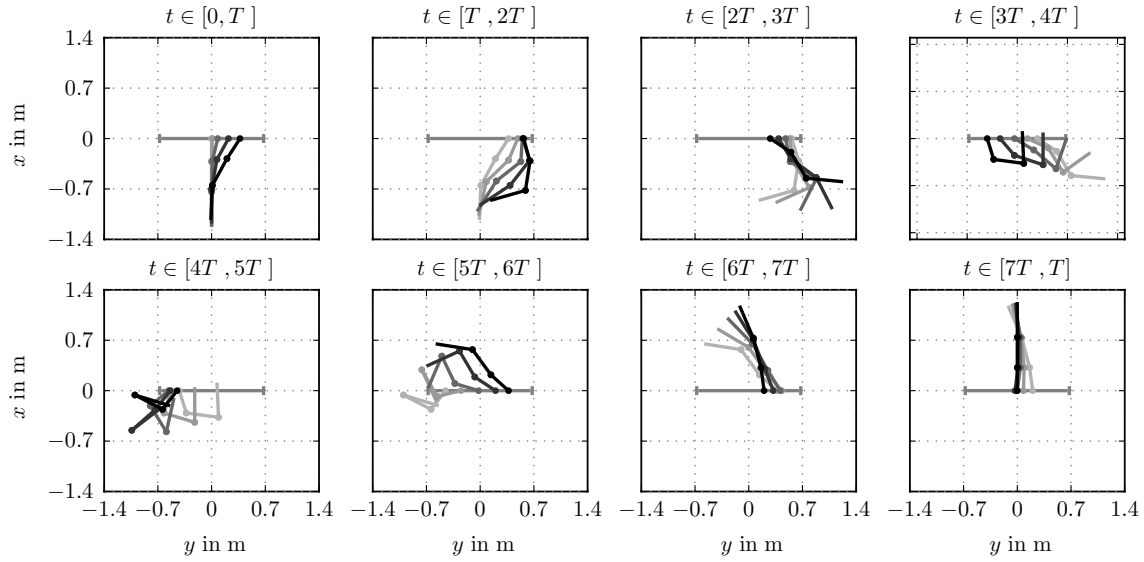

Figure 7. Swing-up maneuver with the transition time $T = 3.5\,\mathrm{s}$.

4.3 Feedback controller and observer design

The previous section was concerned with the feedforward control design. This section presents the development of a stabilizing state feedback controller.

4.3.1 State space formulation and linearization

For the subsequent controller design, the system (5) is linearized along the desired trajectory $(\mathbf{x}^*)^\mathsf{T}(t) = \begin{bmatrix}\mathbf{q}^*(t) & \dot{\mathbf{q}}^*(t)\end{bmatrix}$. In this context, a trajectory of the system (5) for an input $u^*(t)$ with initial condition $\mathbf{x}_0^* = \mathbf{x}^*(0)$ will be denoted by $\mathbf{x}^*(t)$. For sufficiently small deviations from the desired nominal trajectory $\mathbf{x}(t) = \mathbf{x}^*(t) + \Delta\mathbf{x}(t)$, $y(t) = y^*(t) + \Delta y(t)$ and $u(t) = u^*(t) + \Delta u(t)$, the system (5) can be described by the linear, time-variant state space formulation

$$\begin{aligned} \Delta\dot{\mathbf{x}} &= \mathbf{A}(t)\Delta\mathbf{x} + \mathbf{b}(t)\Delta u, \quad \Delta\mathbf{x}(t_0) = \Delta\mathbf{x}_0 \\ \Delta y &= \mathbf{c}^\mathsf{T}\Delta\mathbf{x}, \end{aligned} \tag{27}$$

with $\Delta\mathbf{x}_0 = \mathbf{x}_0 - \mathbf{x}_0^*$ and system matrix and input vector

$$\mathbf{A}(t) = \frac{\partial}{\partial\mathbf{x}}\left(\mathbf{f}(\mathbf{x}) + \mathbf{g}(\mathbf{x})u\right)\Big|_{\mathbf{x}=\mathbf{x}^*(t),u=u^*(t)}, \tag{28a}$$

$$\mathbf{b}(t) = \boldsymbol{g}(\mathbf{x}^*(t)). \tag{28b}$$

Post-print version of the article: T. Glück, A. Eder, and A. Kugi, "Swing-up control of a triple pendulum on a cart with experimental validation", *Automatica*, vol. 49, no. 3, pp. 801–808, 2013. DOI: 10.1016/j.automatica.2012.12.006
The content of this post-print version is identical to the published paper but without the publisher's final layout or copy editing.

A simple numerical integration by means of the *Euler-method*, see, e.g., [16], is utilized to calculate the time-discrete system representation (29) for the sampling time T_a in the form

$$\begin{aligned} \Delta\mathbf{x}_{k+1} &= \mathbf{\Phi}_k \Delta\mathbf{x}_k + \mathbf{\Gamma}_k \Delta u_k, \quad \Delta\mathbf{x}(t_0) = \Delta\mathbf{x}_0, \\ \Delta y_k &= \mathbf{c}^\mathsf{T} \Delta\mathbf{x}_k, \end{aligned} \tag{29}$$

with $\Delta\mathbf{x}_k = \Delta\mathbf{x}(kT_a)$, $\Delta u_k = \Delta u(kT_a)$, $\Delta y_k = \Delta y(kT_a)$, $\mathbf{\Phi}_k = \mathbf{I}_{8\times 8} + T_a\,\mathbf{A}(kT_a)$ and $\mathbf{\Gamma}_k = T_a\,\mathbf{b}(kT_a)$, $k \in \mathbb{Z}$.

4.3.2 Time-variant Riccati Controller

In order to compensate for constant perturbations and parameter mismatches, a state controller with integral part

$$\begin{aligned} \Delta x_{I,k+1} &= \Delta x_{I,k} + \left(y_k^* - \mathbf{c}^\mathsf{T}\mathbf{x}_k\right), \quad \Delta x_I(0) = \Delta x_{I,0}, \\ \Delta u_k &= \boldsymbol{k}_k^\mathsf{T} \Delta\mathbf{x}_{e,k}, \end{aligned} \tag{30}$$

with the extended state vector $\Delta\mathbf{x}_{e,k}^\mathsf{T} = \left[\Delta\mathbf{x}_k^\mathsf{T}\ \Delta x_{I,k}\right]$ and the time-variant gain $\boldsymbol{k}_k^\mathsf{T} = \left[\boldsymbol{k}_{x,k}^\mathsf{T}\ k_{I,k}\right]$ was designed. Augmenting the state space formulation (29) with the integrator state from (30) gives rise to the extended system matrix $\tilde{\mathbf{\Phi}}_k$, the extended input vector $\tilde{\mathbf{\Gamma}}_k$ and the extended output vector $\tilde{\boldsymbol{c}}^\mathsf{T}$. With this, the discrete *Riccati equation*, see, e.g., [4],

$$\mathbf{P}_k = \left(\mathbf{Q} + \tilde{\mathbf{\Phi}}_k^\mathsf{T}\mathbf{P}_{k+1}\tilde{\mathbf{\Phi}}_k\right) + \left(\tilde{\mathbf{\Gamma}}_k^\mathsf{T}\mathbf{P}_{k+1}\tilde{\mathbf{\Phi}}_k\right)^\mathsf{T} \boldsymbol{k}_k^\mathsf{T}, \tag{31a}$$

$$\boldsymbol{k}_k^\mathsf{T} = -\left(\rho + \tilde{\mathbf{\Gamma}}_k^\mathsf{T}\mathbf{P}_{k+1}\tilde{\mathbf{\Gamma}}_k\right)^{-1} \tilde{\mathbf{\Gamma}}_k^T\mathbf{P}_{k+1}\tilde{\mathbf{\Phi}}_k \tag{31b}$$

with $\mathbf{P}_{N+1} = \mathbf{\Lambda}$ was solved to calculate the time-variant gain $\boldsymbol{k}_k^\mathsf{T} \in \mathbb{R}^9$, $k = 0, \ldots, J$ with $J = T/T_a$. Herein, $\mathbf{P}_k \in \mathbb{R}^{9\times 9}$ is symmetric and positive definite, $\mathbf{Q} \in \mathbb{R}^{9\times 9}$ denotes the positive definite weighting matrix of the extended states $\Delta\mathbf{x}_{e,k}$ and $\rho > 0$ is the scalar input weighting factor. The solution $\mathbf{P}_s$ of the discrete algebraic *Riccati equation* ($\mathbf{P}_{k+1} = \mathbf{P}_k = \mathbf{P}_s$) was used as the terminal condition $\mathbf{\Lambda}$ in (31). The controller design parameters are chosen as $\mathbf{Q} = \mathrm{diag}\left(\breve{q}_1\ \breve{q}_2\ \breve{q}_1\ \breve{q}_2\ \breve{q}_1\ \breve{q}_2\ 500\ 20\ 0.01\right)$ with $\breve{q}_1 = 900$, $\breve{q}_2 = 100$ and $\rho = 1000$.

4.4 Observer design

As only the three pendulum angles $\varphi_i, i \in \{1, 2, 3\}$ and the cart position s are measurable, a nonlinear observer was designed to estimate the non-measurable states. Therefore, the design of an *Extended Kalman Filter* is carried out. For this, again the *Euler-method* is applied to (5) to obtain the time-discrete model representation

$$\mathbf{x}_{k+1} = \mathbf{x}_k + T_a\big(\mathbf{f}(\mathbf{x}_k) + \mathbf{g}(\mathbf{x}_k)u_k\big) \approx \mathbf{F}(\mathbf{x}_k, u_k). \tag{32}$$

Taking into account additive zero-mean Gaussian measurement and process noise, $\mathbf{w}_k$ and $\mathbf{v}_k$, with the associated positive definite covariance matrices $\mathbf{S} \in \mathbb{R}^{8\times 8}$ and $\mathbf{R} \in \mathbb{R}^{4\times 4}$, respectively, the following time-discrete nonlinear model

$$\begin{aligned} \mathbf{x}_{k+1} &= \mathbf{F}(\mathbf{x}_k, u_k) + \mathbf{w}_k, \quad \mathbf{x}(0) = \mathbf{x}_0, \\ \mathbf{y}_{m,k} &= \mathbf{C}_m\mathbf{x}_k + \mathbf{v}_k \end{aligned} \tag{33}$$

serves as a basis for the observer design. The measured states are collected in an output vector $\mathbf{y}_m^\mathsf{T} = [\varphi_1\ \varphi_2\ \varphi_3\ s]$ with associated output matrix $\mathbf{C}_m \in \mathbb{R}^{4\times 8}$. The algorithm of the discrete *Extended Kalman Filter*, see, e.g., [1], consists of a prediction and correction step. The *a posteriori* estimate of $\mathbf{x}_k$, taking into account the measurements up to the time kT_a, is denoted by $\hat{\mathbf{x}}_k^+$ and the *a priori* estimate of $\mathbf{x}_k$, taking into account the measurements up to the time $(k-1)T_a$, is denoted by $\hat{\mathbf{x}}_k^-$. In the correction step

$$\begin{aligned} \hat{\mathbf{L}}_k &= \hat{\mathbf{P}}_k^- \mathbf{C}_m^\mathsf{T}\left(\mathbf{C}_m\hat{\mathbf{P}}_k^-\mathbf{C}_m^\mathsf{T} + \mathbf{R}\right)^{-1}, \ \hat{\mathbf{P}}(0) = \hat{\mathbf{P}}_0, \\ \hat{\mathbf{x}}_k^+ &= \hat{\mathbf{x}}_k^- + \hat{\mathbf{L}}_k\left(\mathbf{y}_{m,k} - \mathbf{C}_m\hat{\mathbf{x}}_k^-\right), \quad \hat{\mathbf{x}}(0) = \hat{\mathbf{x}}_0, \\ \hat{\mathbf{P}}_k^+ &= \left(\mathbf{I}_{8\times 8} - \hat{\mathbf{L}}_k\mathbf{C}_m\right)\hat{\mathbf{P}}_k^- \end{aligned} \tag{34}$$

the gain matrix $\hat{\mathbf{L}}_k$ is computed and the *a posteriori* state vector $\hat{\mathbf{x}}_k^+$ and the positive definite covariance matrix of the estimation error $\hat{\mathbf{P}}_k$ is updated by means of the current measurement $\mathbf{y}_{m,k}$. The prediction step

$$\begin{aligned} \mathbf{\Phi}_k &= \left.\frac{\partial}{\partial\mathbf{x}_k}\mathbf{F}\left(\mathbf{x}_k, u_k\right)\right|_{\mathbf{x}_k = \hat{\mathbf{x}}_k^+}, \\ \hat{\mathbf{x}}_{k+1}^- &= \mathbf{F}\left(\hat{\mathbf{x}}_k^+, u_k\right), \ \hat{\mathbf{P}}_{k+1}^- = \mathbf{\Phi}_k\hat{\mathbf{P}}_k^+\mathbf{\Phi}_k^\mathsf{T} + \mathbf{S} \end{aligned} \tag{35}$$

estimates the *a priori* state vector $\hat{\mathbf{x}}_{k+1}^-$ and the covariance matrix of the estimation error $\hat{\mathbf{P}}_{k+1}^-$ at the time instant $(k+1)T_a$. The observer design parameters are chosen as $\mathbf{S} = \mathrm{diag}\left(s_1\ s_2\ s_1\ s_2\ s_1\ s_2\ s_1\ s_2\right)$ with $s_1 = 50$ and $s_2 = 500$, $\mathbf{R} = \mathrm{diag}\left(5\,5\,5\,4\right)$, $\mathbf{P}_0 = 100\mathbf{I}_{8\times 8}$ and $\hat{\mathbf{x}}_0 = \mathbf{x}_0$.

5 Experimental results

Prior to its implementation, the overall swing-up strategy was verified in several simulation studies in MATLAB/SIMULINK. The control strategy was then implemented on the real-time measurement and control system dSPACE DS1103 with a sampling time of $T_a = 1\,\mathrm{ms}$. The desired nominal trajectories $y^*(t), \dot{y}^*(t)$, $\boldsymbol{\eta}^*(t), \dot{\boldsymbol{\eta}}^*(t)$ and the feedforward control $u^*(t) = \ddot{y}^*(t)$ were calculated offline, interpolated at a time grid $t_k = kT_a, k = 0, 1, \ldots, J$ and stored in look-up tables. The same procedure was carried out for the controller gain $\boldsymbol{k}_k$. Figure 8 shows the experimental results and the nominal trajectories as well as the overall control

Post-print version of the article: T. Glück, A. Eder, and A. Kugi, "Swing-up control of a triple pendulum on a cart with experimental validation", *Automatica*, vol. 49, no. 3, pp. 801–808, 2013. DOI: 10.1016/j.automatica.2012.12.006
The content of this post-print version is identical to the published paper but without the publisher's final layout or copy editing.

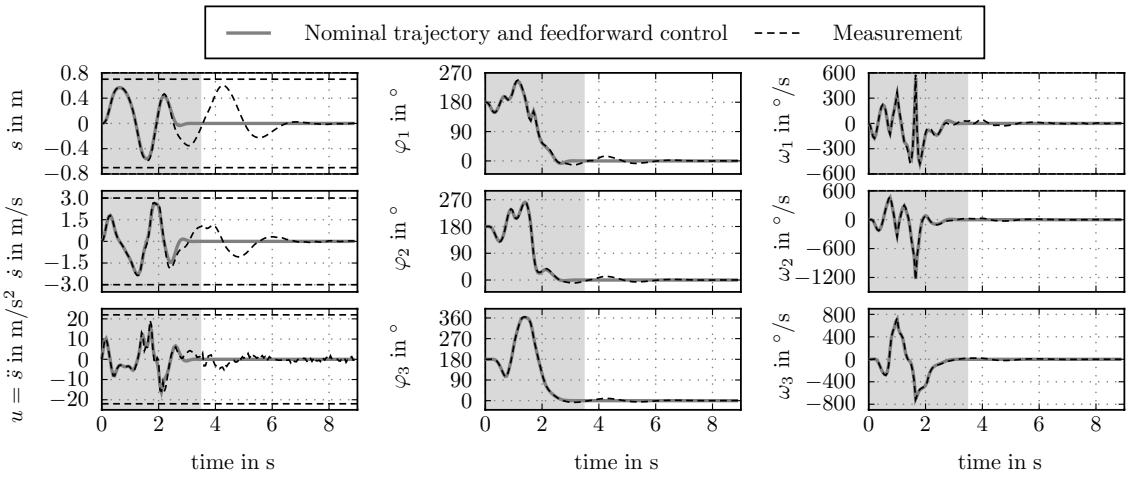

Figure 8. Measurement results for the swing-up maneuver with a transition time of $T = 3.5\,\mathrm{s}$.

of the swing-up maneuver with a transition time of $T = 3.5\,\mathrm{s}$. The time interval $t \in [0, T]$ corresponding to the swing-up trajectory is highlighted in gray. The deviations of the angles and angular velocities from their nominal trajectories are very small. As can be seen from Figure 8, even these small tracking errors result in a position over-shoot of approximately 0.6 m, which illustrates the high sensitivity of the system with respect to control errors. Nonetheless, the cart position, velocity and acceleration comply with their physical constraints and the swing-up maneuver can be successfully accomplished. As already mentioned in the introduction, a video of exactly this swing-up maneuver is made available on `http://www.acin.tuwien.ac.at/fileadmin/cds/videos/TP_Swing_up.wmv`

6 Conclusion

The presented work deals with the swing-up of the triple pendulum on a cart. The swing-up maneuver is accomplished within a two-degrees-of-freedom control scheme consisting of a nonlinear feedforward controller and an optimal feedback controller. Based on a precise mathematical model, the feedforward controller was obtained by solving a nonlinear two-point boundary value problem with free parameters. A time-variant *Riccati Controller* was developed in order to stabilize the system along the nominal trajectory and an *Extended Kalman Filter* was used to estimate the non-measurable states. The overall control strategy for the swing-up maneuver was successfully implemented and tested on an experimental test bench. Up to the authors' knowledge, this is the first contribution so far providing numerical and experimental results of the swing-up maneuver for a triple pendulum on a cart.

References

[1] B.D.O. Anderson and J.B. Moore. *Optimal filtering*. Prentice-Hall, Englewood Cliffs, 1979.

[2] M.J. Anderson and W.J. Granthman. Lyapunov optimal feedback control of a nonlinear inverted pendulum. *Journal of Dynamic Systems, Measurement, and Control*, 111(4):554–558, 1989.

[3] K. G. Eltohamy and C. Y. Kuo. Real time stabilization of a triple link inverted pendulum using single control input. In *Proc. of IEE Control Theory & Applications*, volume 144(5), pages 498–504, 1997.

[4] G.F. Franklin, J.D. Powell, and M.L. Workman. *Digital control of dynamic systems*. Addison-Wesley, 3rd edition, 1997.

[5] K. Graichen. *Feedforward control design for finite-time transition problems of nonlinear systems with input and output constraints*. Shaker Verlag, Aachen, 2006.

[6] K. Graichen, M. Treuer, and M. Zeitz. Fast side-stepping of the triple inverted pendulum via constrained nonlinear feedforward control design. pages 1096–1101, Seville, Spain, Dec. 12-15, 2005. In Proc. of the 44th IEEE Conference on Decision and Control, & the European Control Conference.

[7] K. Graichen, M. Treuer, and M. Zeitz. Swing-up of the double pendulum on a cart by feedforward and feedback control with experimental validation. *Automatica*, 43(1):63–71, 2005.

[8] C.I. Huang and L.C. Fu. Passivity based control of the double inverted pendulum driven by a linear induction motor. In *Proc. of the IEEE International Conference of Control Applications (CCA)*, pages 797–802, Istanbul, Turkey, June 23-25, 2003.

[9] A. Isidori. *Nonlinear control systems*. Springer, Berlin, 1995.

[10] J. Kierzenka and L.F. Shampine. A bvp solver that

Post-print version of the article: T. Glück, A. Eder, and A. Kugi, "Swing-up control of a triple pendulum on a cart with experimental validation", *Automatica*, vol. 49, no. 3, pp. 801–808, 2013. DOI: 10.1016/j.automatica.2012.12.006
The content of this post-print version is identical to the published paper but without the publisher's final layout or copy editing.

controls residual and error. *Journal of Numerical Analysis, Industrial and Applied Mathematics*, 3(1-2):27–41, 2008.

[11] L. Ljung. *System identification: Theory for the user*. Prentice Hall PTR, New Jersey, 1999.

[12] G.A. Medrano-Cerda. Robust stabilization of a triple inverted pendulum-cart. *International Journal of Control*, 68(4):849–865, 1997.

[13] S. Mori, H. Nishihara, and K. Furuta. Control of unstable mechanical systems - control of pendulum. *International Journal of Control*, 23(5):673–692, 1976.

[14] J. Rubí, Á. Rubio, and A. Avello. Swing-up control problem for a self-erecting double inverted pendulum. In *Proc. of the IEE Control Theory & Applications*, volume 149(2), pages 169–175, 2002.

[15] M. Spong and M. Vidyasagar. *Robot dynamics and control*. John Wiley & Sons, New York, 1989.

[16] J. Stoer and R. Burlisch. *Introduction to Numerical Analysis*. Springer, New York, 2002.

[17] Hasomed GmbH. www.hasomed.de, Access: 10.02.2012.

[18] V. A. Tsachouridis. Robust control of a triple inverted pendulum. In *Proc. of the IEEE International Control Applications Conference*, volume 2, pages 1235–1240, Denver, USA, Sept. 28-30, 1235–1240.

[19] M. Wicklund, A. Kristenson, and K.J. Åström. A new strategy for swinging up an inverted pendulum. In *Proc. of the 12th IFAC World Congress*, volume 9, pages 151–154, Sydney, Australia, July 19-23, 1993.

[20] K. Yoshida. Swing-up control of an inverted pendulum by energy-based methods. In *Proc. of the American Control Conference*, volume 6, pages 4045–4047, San Diego, USA, Jun 2-4, 1999.

[21] L. Zhang and Y. Tu. Research of car inverted pendulum model based on lagrange equation. In *Proc. of the 6th World Congress on Intelligent Control and Automation*, volume 1, pages 820–824, Dalian, China, June 21-23, 2006.

[22] W. Zhong and H. Rock. Energy and passivity based control of the double inverted pendulum on a cart. In *Proc. of the IEEE International Conference Applications (CCA)*, volume 1, pages 896–901, Mexico City, Mexico, Sept. 5-7, 2001.

Post-print version of the article: T. Glück, A. Eder, and A. Kugi, "Swing-up control of a triple pendulum on a cart with experimental validation", *Automatica*, vol. 49, no. 3, pp. 801–808, 2013. DOI: 10.1016/j.automatica.2012.12.006
The content of this post-print version is identical to the published paper but without the publisher's final layout or copy editing.